Stochastic dynamics of penetrable rods in one dimension: Occupied volume and spatial order

Cite as: J. Chem. Phys. **138**, 244901 (2013); https://doi.org/10.1063/1.4810807
Submitted: 08 March 2013 . Accepted: 23 May 2013 . Published Online: 24 June 2013

Galen T. Craven, Alexander V. Popov, and Rigoberto Hernandez

Stochastic dynamics of penetrable rods in one dimension: Occupied volume and spatial order

Galen T. Craven, Alexander V. Popov, and Rigoberto Hernandez[a)]
Center for Computational and Molecular Science and Technology, School of Chemistry and Biochemistry, Georgia Institute of Technology, Atlanta, Georgia 30332-0400, USA

(Received 8 March 2013; accepted 23 May 2013; published online 24 June 2013)

The occupied volume of a penetrable hard rod (HR) system in one dimension is probed through the use of molecular dynamics simulations. In these dynamical simulations, collisions between penetrable rods are governed by a stochastic penetration algorithm (SPA), which allows for rods to either interpenetrate with a probability δ, or collide elastically otherwise. The limiting values of this parameter, $\delta = 0$ and $\delta = 1$, correspond to the HR and the ideal limits, respectively. At intermediate values, $0 < \delta < 1$, mixing of mutually exclusive and independent events is observed, making prediction of the occupied volume nontrivial. At high hard core volume fractions ϕ_0, the occupied volume expression derived by Rikvold and Stell [J. Chem. Phys. **82**, 1014 (1985)] for permeable systems does not accurately predict the occupied volume measured from the SPA simulations. Multi-body effects contribute significantly to the pair correlation function $g_2(r)$ and the simplification by Rikvold and Stell that $g_2(r) = \delta$ in the penetrative region is observed to be inaccurate for the SPA model. We find that an integral over the penetrative region of $g_2(r)$ is the principal quantity that describes the particle overlap ratios corresponding to the observed penetration probabilities. Analytic formulas are developed to predict the occupied volume of mixed systems and agreement is observed between these theoretical predictions and the results measured from simulation. © *2013 AIP Publishing LLC*. [http://dx.doi.org/10.1063/1.4810807]

I. INTRODUCTION

Atoms and molecules can be treated as overlapping particles when soft interaction potentials allow them to partially penetrate through each other relative to their van der Waals distances. But the centers of atoms—nuclei—are not considered to be transparent in all-atom models and thus pairwise interaction potentials that seek to capture this condition of nuclear non-transparency are infinite valued at the origin. When a coarse-grained description of the atomic degrees of freedom is applied, it is often useful to simulate nuclear transparency using a class of potentials that are finite valued at the origin. These potentials have been termed bounded potentials and have been useful in modeling many soft matter and colloidal systems.[1–4]

A well-known bounded potential is the generalized Gaussian core (GGC) model,[5]

$$V^{\mathrm{GGC}}(r) = \epsilon \exp\left[-\left(\frac{r}{\sigma}\right)^n\right]. \tag{1.1}$$

For the exponential parameter value $n = 2$, the GGC takes the form of the Gaussian core (GC) model first introduced by Stillinger.[6] The phase behavior of the GC model has recently been studied[7,8] along with the thermodynamic properties.[9] In the limit of $n \to \infty$, the Gaussian core acquires a piecewise form of a penetrable sphere (PS) model of interactions between solvated micelles, introduced by Marquest and Whitten,[10]

$$V^{\mathrm{PS}}(r) = \begin{cases} 0, & r > \sigma, \\ \epsilon, & r \leq \sigma, \end{cases} \tag{1.2}$$

where σ represents the length of the particles. The structural and thermodynamical properties of the PS model have attracted significant attention,[11–16] in part due to the model's simplicity. This completely repulsive potential has been extended to include attractive sections[17–19] for the purpose of modeling thermodynamic and phase behavior of more complex fluids.

Molecular dynamics (MD) simulations have been performed using the PS potential,[20] and the results have been used to predict the occupied volume fraction, as well as static and transport properties of the PS systems. The hard edges of the PS potential, given by Eq. (1.2), facilitates the study of the volume occupied by overlapping particles (the particle phase). Measuring the occupied volume and surface area of hard-edged overlapping objects is also of interest in studies of the microstructure of porous media[21–24] in which the underlying systems often exhibit permeable behavior.

A characteristic of overlapping hard-edge systems is that the geometric properties can be obtained readily using either analytic studies[25–28] or simulations.[29–32] The (analytic) geometric analysis relies on discrete identification of positions as either being associated with a particle or a void. In soft (or continuous) potentials, such identification is ill-defined and hence the analytic treatments are not applicable.

Blum and Stell[33] introduced a generalized model, called the permeable-sphere model (PSM), with a one parameter

a)Author to whom correspondence should be addressed. Electronic mail: hernandez@chemistry.gatech.edu.

bridge between the hard core and ideal behavior. Namely, the pair correlation function $g_2(r)$ between two particles is assumed to be constant at $r < \sigma$,

$$g_2(r) = 1 - \lambda, \tag{1.3}$$

where λ is the "permeability parameter." The values $\lambda = 1$ and $\lambda = 0$ correspond to the hard sphere and ideal gas behavior, accordingly. Note that a potential in the form of Eq. (1.2) does not automatically lead to a constant value of $g_2(r)$ at $r < \sigma$. This model provides impetus for the system studied in this article.

The stochastic penetration algorithm (SPA), introduced in this article and described in detail in Sec. II A, is another approach for modeling penetrative particles in which collisions are governed by stochastic rules. In future work, we seek to understand how explicit solvent geometries affect reactive systems in solution. By changing the outcomes of stochastic collision events, the SPA allows variation of coupling strength between solvent and solute. While the SPA is an abstraction of a physical system, the results obtained using this model can be used to represent and predict the behavior of coarse-grained solvents where hard-edge boundaries are representative of the physical solvent geometries.

Stochastic collision rules have been used previously in, for example, Lorentz gas systems.[34–37] Therein, the collision with a fixed scatterer can lead either to the reflection of the colliding particle or the transmission of the particle through the scatterer, subject to the outcome of a stochastic variable. These stochastic models have provided analytic insight that was previously unavailable from purely deterministic models. Within the framework of the SPA, a random process—consistent with a given probability—assigns each event between a pair of particles as being entirely penetrable or hard sphere. The nature of the interaction remains the same as long as the pair remains within some distance of each other, and this continuous time interval defines a given event.

Hard-body systems are known to capture the properties of simple fluids[38] and thus they remain a current research topic for both equilibrium and non-equilibrium systems.[39–41] We utilize the SPA to extend the accessible range of pairwise interactions beyond hard spheres while reducing the dimensionality to one for simplicity. This study of hard spheres—hard rods (HRs) in one dimension—is an obvious simplification of the 3D picture but does give insight into the physical properties of more physically realizable systems. The equation of state (EOS) for a bounded one-dimensional HR system has been completely solved by Tonks.[42] This solution has given insight into hard core systems in dimensionalities greater than one, where closed form solutions to the EOS are not available.[43] Analogously, by mixing reflective and penetrative collision outcomes, the SPA model can be used to mathematically elucidate the properties of bounded penetrable systems to a larger extent than is currently available for deterministic bounded potentials. In this way, the SPA can be considered pseudo-soft as the pairwise potential is a mix of completely hard and completely soft interactions, but the mixing of these interactions creates ensemble properties that resemble properties obtained using soft-bounded potentials, such as the PS model, exclusively. In the SPA, the momentum distribution of the system is conserved and thus an analytical analysis can be greatly simplified. The results of these analytical treatments can be used to gain insight into the dynamical and static properties of physical systems that can be represented by such models.

The paper is outlined as follows: In Sec. II A, we describe the SPA with a stochastic collision rule for HRs constrained to move on a line in one dimension. Using this stochastic collision model we are able to change, through a parameter δ, the softness in the underlying interactions within the particle ensemble and thus bridge the behavior between the limits of impenetrable hard particles and completely-soft (ideal) particles. In Sec. II B, the computational problem of measuring the occupied volume fraction is discussed and a simple solution applicable in one dimension is given. Section III includes derivations of theoretical expressions for the occupied volume fraction of stochastically penetrable particles. The dependence of these expressions on the radial distribution function $g_2(r)$ is discussed and the results from theory are compared to the results measured from MD simulations. The structural properties of stochastic models measured from simulation are presented and the disordered structure inherent within these stochastic penetration models is discussed. In Sec. IV, we discuss the results obtained for the occupied volume fraction and the structural properties along with possible future applications of the SPA.

II. NUMERICAL METHODS

A. Model and simulation details of the SPA

MD simulations have been performed on a system of $N = 20$ rods with each particle having a length $\sigma = 3$ Å and mass $m = 14\ m_u$ (m_u is the atomic mass unit). These particles are constrained to move in one dimension on a line of length L_x, with periodic boundary conditions. The HR volume fraction $\phi_0 = N\sigma/L_x$ is the occupied volume fraction of the system when no particles overlap. In the case when the particles can overlap each other, the actual volume fraction ϕ does not exceed the HR one, $\phi \leq \phi_0$.

The values of the particle number density $\rho = N/L_x$ and ϕ_0 are changed by varying the value of L_x while keeping N constant. The HR volume fractions chosen for the study are $\phi_0 \in \{0.125, 0.25, 0.5, 0.75, 0.968\}$. A Tonks gas does not exhibit a phase transition[44] and therefore the system remains in the fluid phase within this range of volume fractions (a fluid-solid phase transition occurs for hard core systems only in dimensions greater than one).

To account for penetrability of the particles in the SPA, we introduce a single bridge parameter δ, analogous to the bridging parameter used by Blum and Stell[33] for their PSM, Eq. (1.3). The limiting values of this parameter, $\delta = 0$ and $\delta = 1$, correspond to the HR and the ideal behavior limits, respectively.

Algorithmically, the SPA is implemented as follows. For every molecular dynamics trajectory, a value of the penetration probability $\delta \in [0, 1]$ is preassigned and maintained throughout the trajectory. When a pair of particles i and j collide at time t_{col}, a random number $a_{ij}(t_{\text{col}}) \in [0, 1]$ is generated from a uniform distribution. This random number

determines, upon its comparison to δ, whether or not the pair of rods will interact. If $a_{ij}(t_{\rm col}) > \delta$, the rods interact via a hard core potential; otherwise the particles penetrate each other without interacting, and the spatial correlation between them vanishes. This lack of spatial correlation corresponds to pairwise ideal behavior. For $\delta = 1$, spatial correlation is removed for all pairs and the dynamics of the system of rods are completely ideal. For $\delta = 0$, all pairwise interactions are governed by a hard core potential and the dynamics observed are that of a Tonks gas, a system of HRs confined to move on a line in one dimension. For the overlapping particles which do not interact, this relationship between $a_{ij}(t_{\rm col})$ and δ is maintained until $r_{ij} > \sigma$, i.e., the zero interaction potential is kept until the pair breaks apart. If the same pair of particles (i, j) undergoes a new collision at time $t_{\rm col} + \tau$, then a new random number $a_{ij}(t_{\rm col} + \tau)$ is generated and the acceptance algorithm is repeated. This algorithm is used to construct all pairwise interactions in the SPA simulations. The corresponding potential between particles i and j is described by the following equation:

$$V_{ij}^{\rm SPA}(r) = \begin{cases} 0, & r > \sigma, \\ 0, & r \le \sigma \ \text{ and } \ a_{ij}(t_{\rm col}) < \delta, \\ \infty, & r \le \sigma \ \text{ and } \ a_{ij}(t_{\rm col}) > \delta. \end{cases} \tag{2.1}$$

The interaction between all particle pairs can be represented by undirected network graphs with each node corresponding to a specific particle. For a system of N particles, there are $N(N-1)/2$ possible connections associated with the pairwise interactions—HR at $\delta = 0$ or penetrative at $\delta = 1$. Figure 1 shows representative graphs of different configurations that can be observed using the SPA. As the system evolves in time, connections can be made and broken due to the stochastic nature of the SPA allowing for a sampling of different network configurations. For both a Tonks and an ideal gas, the spatial boundaries for every particle can be calculated from knowledge of the connection network.

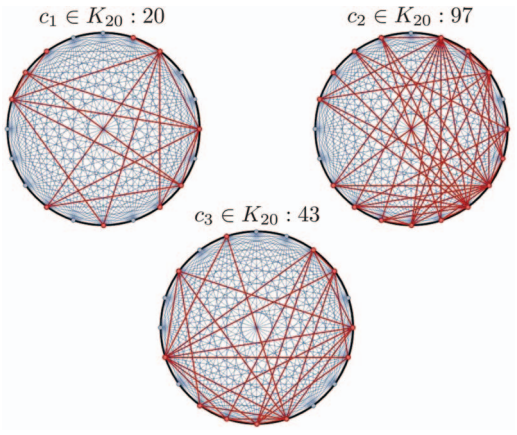

FIG. 1. Representative graphs for a system consisting of $N = 20$ particles, showing different configurations of the connection network. Each graph node located on the circumference of the circle corresponds to a different particle. The lines represent the complete graph K_N – all the $N(N-1)/2$ theoretically possible connections available for a system. Lines are colored in red or blue depending on if they correspond to an activated HR connection or a non-activated connection, respectively. The network with j activated connections is denoted as K_N: j. The configuration c_k is an element of the possible set of permutations for a K_N: j network.

These boundaries define the configuration integral and lead to closed form solutions of the partition functions. The equilibrium thermodynamic properties for these systems are consequently also contained in these types of connection networks. They can be extracted directly from the graphs in Fig. 1 and the corresponding adjacency matrices used to construct them.

To propagate the dynamics of the SPA, the particle positions and velocities are updated through a combination of the time-driven method and the well-known hard-sphere algorithm.[45] Note that at the time of a given collision between two particles, their velocities are exchanged as the collision is elastic and the particles have equal masses. In other words, the velocity distribution is conserved during the evolution of the system, in contrast with the PS model and other models in which particle interactions are governed by soft potentials.

The initial positions for the particles are chosen by placing their centers on a uniform lattice. The initial velocities are sampled randomly from a Maxwellian distribution corresponding to $T = 300$ K. For each value of δ and ϕ_0, 8000 trajectories have been simulated for a time of 1000 ps. The simulations are partitioned into three phases: an initial spatial and thermal equilibration phase, a second spatial relaxation regime, and a sampling phase.

During the first phase, lasting 12.5 ps, all interactions between particles are represented by HR potentials. After the initial velocities are assigned, these velocities are rescaled such that the total energy of the system, for every trajectory, corresponds to $T = 300$ K. This thermal equilibration step is achieved by measuring the kinetic temperature,

$$T_m = \frac{m}{N k_B} \sum_{i=1}^{N} v_i^2, \tag{2.2}$$

and scaling the velocity of each particle using the equation

$$v_i' = v_i \sqrt{\frac{T}{T_m}}. \tag{2.3}$$

After one such rescaling the kinetic energy of the system becomes $NkT/2$. Since all collisions are elastic, all the energy of the system partitioned into the kinetic term is constant. The conservation of energy implies that these simulations take place in a microcanonical (NVE) ensemble with the kinetic energy corresponding to 300 K. Although for the HR interaction, it is not necessary to perform the rescaling procedure during 12.5 ps, we keep this operation in the code for future studies employing soft potentials.

The second equilibration phase is performed until the total simulation time reaches 500 ps. During this phase, the SPA algorithm is applied, allowing particles to overlap. Figure 2 shows different spatial configurations of overlapping particles that can be observed for a penetrable HR system. Note that the connection network K_N: j, presented in Fig. 1, does not specify the spatial arrangement of a set of overlapping particles as a given spatial configuration can be generated by many such networks.

As illustrated in Fig. 2, the volume fraction ϕ is reduced from its initial value ϕ_0 as the rods interpenetrate. The geometry of the system, as well as the distribution of free volume cavities, can be significantly altered by this penetration. As

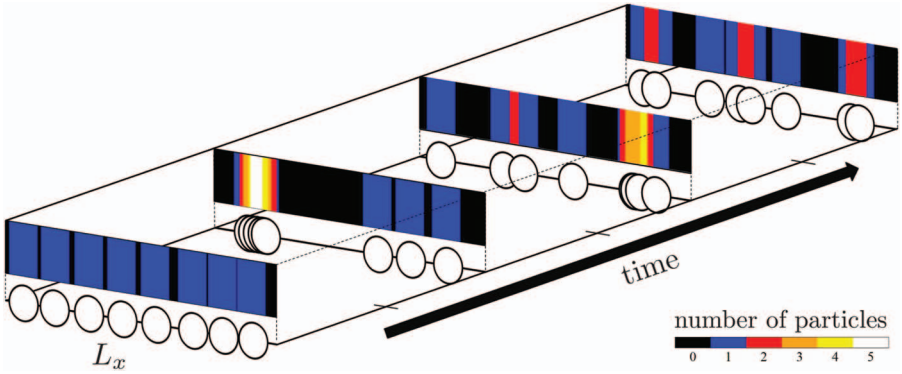

FIG. 2. Several snapshots of configurations that 8 particles can take as opposed to the 20 particles in Fig. 1. The connection network of this 8 particle system can be represented by the complete graph K_8. The network evolves through different connection networks $c_1 \rightarrow c_2 \rightarrow c_3 \rightarrow c_4$, respectively, illustrating how the observed volume fraction $\phi(t)$ starts with ϕ_0 and then changes with time due to particle overlaps.

shown in Fig. 3, the relaxation of ϕ is fast and the measured volume fraction is seen to relax to its equilibrium value during this second equilibration phase.

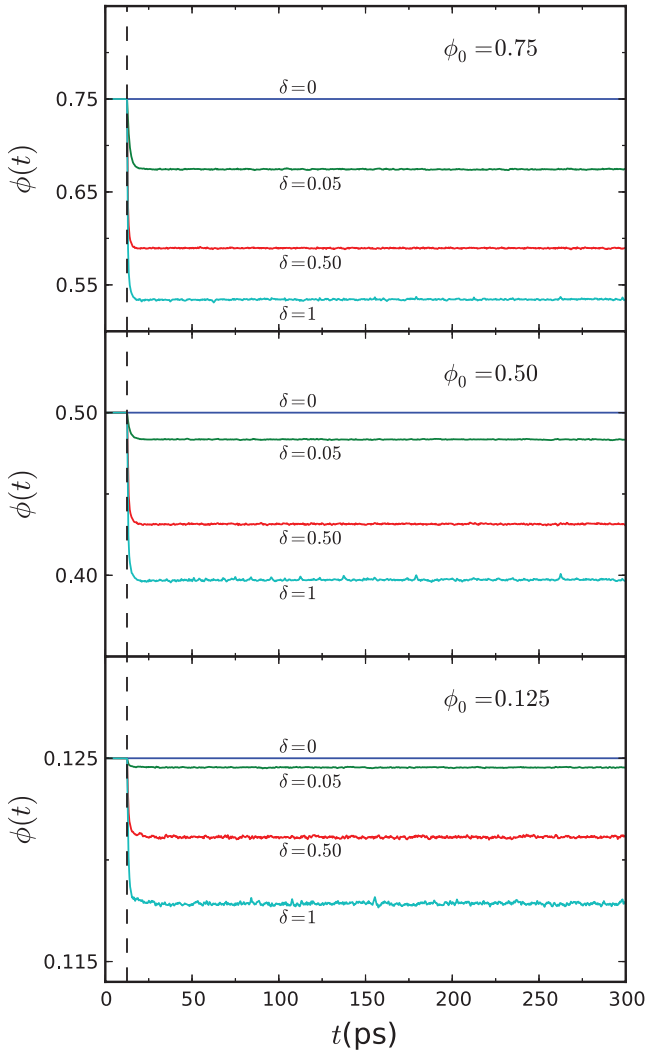

FIG. 3. The measured volume fraction $\phi(t)$ as a function of time showing the fast relaxation to equilibrium for various values of the hard rod volume fraction ϕ_0 and the penetration probability parameter δ. Although labeled, the curves are also indicated in color as blue, green, red, and cyan for values of δ equal to 0, 0.05, 0.5, and 1, respectively. The dashed vertical line corresponds to the time (12.5 ps) at which the penetration algorithm begins.

After two initial equilibration stages, sampling of the equilibrium values of the system is performed up to $t = 1000$ ps. During this sampling phase, the spatial coordinates of the system were written to disk every 0.1 ps and ensemble averaging of these trajectory frames was used in calculating all observable quantities presented in this article.

B. Measurement of the occupied volume fraction

The determination of the occupied volume of systems with overlapping particles is non-trivial and can be computationally expensive if exact methods are not applicable. Two methods that have been used previously to measure the occupied volume are Monte Carlo (MC) integration[30,46] and the so-called GRID method.[20,29,30]

The brute force MC approach, analogous to simple MC integration procedures, involves choosing a random spatial coordinate and checking if that coordinate is overlapped by a particle from the system. Unfortunately, the computational cost of the MC method makes it intractable for integration of a high number of trajectory frames when a large number of significant figures is needed.

In the GRID method, a sample space is first discretized into a set number of bins. These bins are then probed individually to see if any particle overlaps with the chosen bin. For a hypercubic structure in dimension D, discretization of the one-dimensional length L_x into k bins scales as k^D. Lee and Torquato[30] extended this simplistic one length scale discretization approach by further subdividing a bin if it contains two phases: the particle phase and the void phase. That is, if a particle edge overlaps a given bin, then the bin is subdivided into smaller ones and the procedure is repeated in the subdivided space. As the size of the grid goes to zero, the exact measure of the occupied volume will be obtained. However, the computational cost of this method is also high.

To overcome this computational problem, a cluster measure approach has been applied for calculating the volume fraction. A cluster is defined as a formation consisting of $N \geq 1$ particles (thus, a single particle can be termed a cluster). For a set of N particles, there exist a maximum of N clusters, corresponding to a configuration where no particles are overlapped, and a minimum of one cluster, corresponding to the

configuration where all of the particles are overlapped into a single cluster. In one dimension, it is simple to determine the beginning and end points, x^{begin} and x^{end}, of these clusters along the line segment L_x. After ordering the particles, ϕ can be found by summing the sizes of all the (nonoverlapping) clusters

$$\phi = \frac{1}{L_x} \sum_{i=1}^{\text{all clusters}} \left(x_i^{\text{end}} - x_i^{\text{begin}}\right). \tag{2.4}$$

This method gives no measurement error and is accurate to floating point precision. Some other cluster-based algorithms have been proposed for two-dimensional systems.[47] If comparably efficient algorithms can be applied in higher dimension, large increases in computational efficiency could be observed for other models where there is overlap in one phase of the media and a measure of occupied volume is computationally taxing. The simulation cost of HR systems far from the thermodynamic limit, like the systems presented in this article, is negligible compared to the computation time of post-processing the trajectories and, thus, using the cluster measure method greatly accelerates the rate of data acquisition and analysis.

III. THEORY AND RESULTS

A. Spatial order

The HRs with initial positions placed on a periodic lattice will oscillate about those lattice points with some approximate frequency that is dependent on the velocity distribution. To verify that a HR system has reached an equilibrium spatial configuration, it is common to wait until the measured pressure becomes equal to the equilibrium one[48] as the equation of state for a HR system is known exactly.[42] For SPA dynamics, the equation of state is known only for the limiting values of δ and therefore this method of equilibration verification is not available.

According to Haus and Raveché,[49] the translational order parameter,

$$f(t) = \frac{1}{N} \sum_{i=1}^{N} \cos\left(2\pi\rho x_i\right), \tag{3.1}$$

acquires its equilibrium value if a HR system with concentration $\rho = N/L_x$ reaches equilibrium. As discussed in Ref. 49, $f(t) = 1$ for a crystalline array where particles do not move from their original lattice positions. For an ordered configuration $f(t)$ fluctuates about a non-zero value, and for a random configuration $f(t)$ fluctuates about zero. For a system with periodic boundary conditions, the center-of-mass coordinate x_{com} moves with a slow constant velocity v_{com}. By accounting for the center-of-mass translation of the lattice points, we define a shifted translational order parameter,

$$h(t) = \frac{1}{N} \sum_{i=1}^{N} \cos\left(2\pi\rho\left(x_i - x_{\text{com}}\right)\right). \tag{3.2}$$

Figure 4 shows the time evolution of $h(t)$ using SPA dynamics. The spatial structure persists only at the extremes, i.e., for the most ordered ($\delta = 0$) and dense ($\phi_0 = 0.75$ and 0.968)

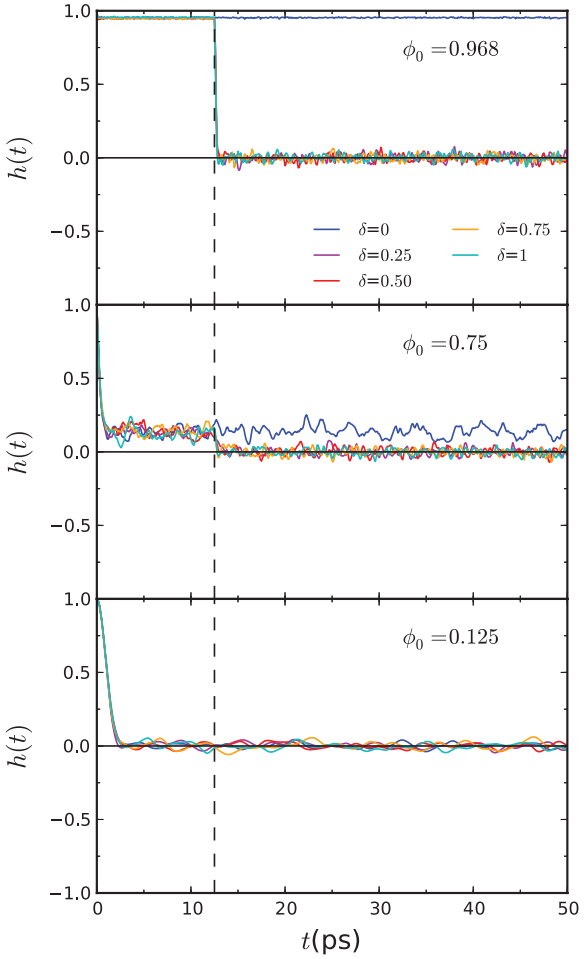

FIG. 4. The shifted translational order parameter $h(t)$ averaged over 50 trajectories. The curves are color coded as in Fig. 3 with the addition of δ equal to 0.25 and 0.75 which are colored in magenta and orange, respectively. The dashed vertical line corresponds to the time (12.5 ps) at which the penetration algorithm begins.

systems. The function $h(t)$ falls quickly to the disordered $h(t) = 0$ value at $\delta > 0$, when particles can overlap each other, thus exchanging their positions on the lattice and causing a degradation of the order.

B. Pair correlation function and the penetration coefficient

Salsburg, Zwanzig, and Kirkwood[50] have derived an exact analytic expression for the radial distribution function $g_2(r)$ for the HR model. This structural prediction has been shown to agree with results obtained through MD simulations.[48,49] MD studies of one-dimensional systems have extended to soft potentials[51] and therefore the numerical results observed for the HR model can be compared to potentials that give some degree of penetration while still remaining unbounded at the origin. Because of the penetrable nature of one-dimensional bounded potentials, complex interaction networks can be created. The presence of these multibody interactions can contribute significantly to the structural and dynamical properties and thus an analytical treatment of such systems is often found to be intractable even in one

dimension. In a SPA system, the interactions are nearest neighbor interactions as particles penetrate each other with no energy cost. As such, the SPA system is sufficiently simple that the thermodynamic and structural properties likely admit to a tractable analytic analysis.

Within the SPA model, the pairwise overlapping probability δ has a significant influence on the form of the pair correlation function (see Fig. 5). The latter, therefore, can include δ as a parameter: $g_2 = g_2(r; \delta)$. An integral of $g_2(r; \delta)$ over the penetration region,

$$\zeta(\delta) = \frac{1}{\sigma}\int_0^{\sigma} g_2(x;\delta)\,dx, \tag{3.3}$$

defines the multi-body induced probability to find a particle at $r < \sigma$ and, in general, is not equal to δ, opposite to the PSM, Eqs. (1.3), where it is postulated (see also Eq. (3.5) below). Figure 5 illustrates the fact that the pair correlation function approaches constant behavior for $r < \sigma$ only when ϕ_0 is small. At higher ϕ_0 values, the penetrative region indicated by $g_2(r; \delta)$ is nonlinear. Observation that $g_2(0; \delta) \geq g_2(\sigma^-; \delta)$ (σ^- represents approaching the discontinuity at $r = \sigma$ from the left) with the equality holding only for the limiting values of δ and at infinite dilution shows a propensity for the particles to be heavily overlapped in a volume reducing state. This reduced volume state can be explained thermodynamically by noting that it is favorable for a system to be in a state that reduces the pressure. For a cluster of $N \geq 2$ particles, the particles in the cluster are free to overlap each other with no energy cost as given by Eq. (2.1). This cluster can be confined between a pair of particles where the confining pair and the cluster interact through HR interactions. When this overlapping cluster is formed, the system moves spontaneously toward a reduced pressure state. The confining particles push on the cluster and this applied pressure forces the cluster into a state that minimizes the occupied volume. This minimization occurs when all the particles in the cluster are completely overlapped and the propensity for complete overlap gives rise to the inequality $g_2(0; \delta) \geq g_2(\sigma^-; \delta)$. At low δ and large ϕ_0, where clusters are likely to be confined, this phenomenon is a prominent feature of $g_2(r; \delta)$, but for high δ values the contribution is not significant.

Figure 6 shows ζ as a function of δ. The ζ values are calculated by numerical integration of Eq. (3.3) for $g_2(r; \delta)$ values obtained from MD simulations. Figure 6 also shows that as the system becomes less dense the overlap ratio approaches the PSM behavior,

$$\lim_{\phi_0 \to 0} \zeta = \delta \tag{3.4}$$

(compare with Eq. (3.5)). As ϕ_0 moves away from this limit, the ratio of ζ to δ also increases, showing that the actual overlap ratios are given by ζ and not δ. The cause of this movement to ideality can be seen in Fig. 5, where $g_2(r; \delta)$ is almost constant for $r < \sigma$ at $\phi_0 = 0.125$.

In applications, the actual penetration coefficient ζ must be used in place of δ to account for multi-body effects.

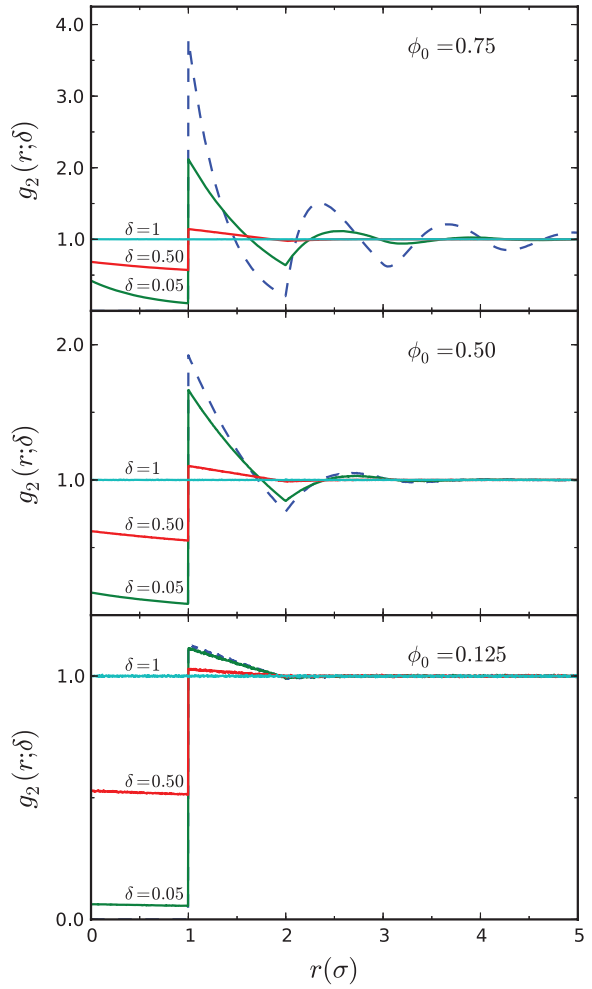

FIG. 5. The pair correlation function $g_2(r; \delta)$ measured from simulations at various ϕ_0 and δ values using a histogram bin width of 0.01σ. The curves are color coded as in Fig. 3. The blue dashed curves correspond to the results obtained for an impenetrable HR system, i.e., when $\delta = 0$.

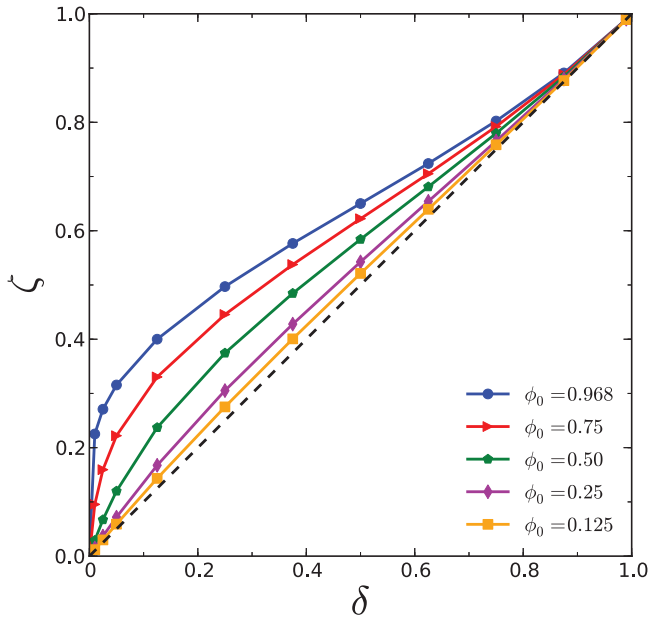

FIG. 6. ζ as a function of δ showing the deviation from ideal behavior for the observed particle overlap ratios. ζ is obtained from simulation using Eq. (3.3). The black dashed line corresponds to the infinite dilution limit, where $\zeta = \delta$.

C. Occupied volume fraction

For the PSM posited by Blum and Stell[33] with a pair correlation function given by Eq. (1.3), the probability δ to find more than one particle in the penetrative region is

$$\delta = \frac{1}{\sigma}\int_0^\sigma g_2(x)dx = 1 - \lambda. \tag{3.5}$$

Rikvold and Stell[52] (RS) used the Kirkwood superposition approximation for a multi-particle correlation function,

$$g_n(\boldsymbol{r}_1, \ldots, \boldsymbol{r}_n) = \prod_{1\le i<j\le n} g_2(r_{ij}), \tag{3.6}$$

to derive the occupied volume fraction of a PSM system:[53,54]

$$\phi_{\text{inf}}^{\text{RS}}(\delta) = -\sum_{k=1}^{\infty} \frac{(-\phi_0)^k}{k!}\delta^{\frac{k(k-1)}{2}} \tag{3.7}$$

(cf. Eq. (8) in Ref. 54), where ϕ_0 is the volume fraction for a HR system consisting of N particles,

$$\phi_0 = \frac{N\sigma}{L_x}. \tag{3.8}$$

At $\delta = 0$, Eq. (3.7) gives the exact value for a HR gas, $\phi_{\text{inf}}^{\text{RS}}(0) = \phi_0$. A limiting value at $\delta = 1$ recovers another exact result for the ideal behavior of fully permeable spheres in the thermodynamic limit ($N \to \infty$, $L_x \to \infty$),

$$\phi_{\text{inf}}^{\text{RS}}(1) = 1 - \exp[-\phi_0]. \tag{3.9}$$

Equation (3.9) is the well known Poisson distributed result[24,55] for the volume fraction of particles with no spatial correlation at the thermodynamic limit. Note that both Eqs. (3.7) and (3.9) are valid for any spatial dimension D.

The RS derivation of the volume fraction for the PSM depends on $g_2(r)$ being constant in the penetrative region. This simplification should give good agreement to simulation results if, in the Ornstein-Zernike formalism, direct contributions between two particles are the dominant terms in $g_2(r)$, while the indirect contributions due to multi-body effects are relatively small.

For finite N, the dimensionally invariant expression for the occupied volume of particles with no spatial correlation is

$$\phi = 1 - \left(1 - \frac{\phi_0}{N}\right)^N. \tag{3.10}$$

It stems from the fact that the probability for one particle not to cover a selected point is $1 - \sigma/L_x = 1 - \phi_0/N$, and for N uncorrelated particles it is $(1 - \phi_0/N)^N$. At $N \to \infty$, Eq. (3.10) acquires the form of Eq. (3.9) – its thermodynamic limit. The difference between these equations lies in the series expansions over ϕ_0,

$$\phi = -\sum_{k=1}^{N} C_k' \phi_0^k, \tag{3.11}$$

whereas

$$\phi_{\text{inf}}^{\text{RS}}(1) = -\sum_{k=1}^{\infty} C_k \phi_0^k. \tag{3.12}$$

The coefficients of these series are

$$C_k' = \binom{N}{k}\frac{(-1)^k}{N^k}, \tag{3.13}$$

and

$$C_k = \frac{(-1)^k}{k!}, \tag{3.14}$$

where $\binom{N}{k}$ is the binomial coefficient. As $N \to \infty$, $C_k' \to C_k$.

Analogously, in the RS formula, Eq. (3.7), with finite N, the exponential power series coefficients C_k must be replaced by the finite series coefficients C_k' to obtain

$$\phi_{\text{fin}}^{\text{RS}}(\delta) = -\sum_{k=1}^{N} \binom{N}{k}\frac{(-\phi_0)^k}{N^k}\delta^{\frac{k(k-1)}{2}}. \tag{3.15}$$

The results given by Eq. (3.15) are compared to the data obtained from MD simulations in Fig. 7. It can be seen that for small $\phi_0 \in \{0.125, 0.25\}$, these results show excellent agreement, but as ϕ_0 is increased, $\phi_{\text{fin}}^{\text{RS}}(\delta)$ deviates significantly from the simulations, especially for small δ. While the RS formula does capture the nonlinear nature of ϕ, it fails to give accurate predictions over all values of ϕ and δ. In Sec. III C 1, we derive an expression which is shown to have excellent agreement with the results obtained from simulation. A second semi-empirical functional form is summarized in the Appendix. This model agrees with the results obtained from MD simulations up to the inclusion of two *ad hoc* (fitting) parameters.

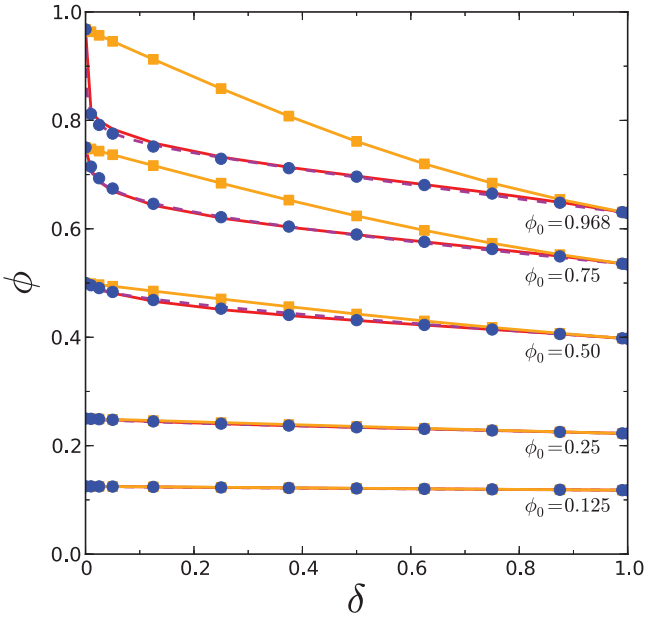

FIG. 7. Occupied volume fraction ϕ as a function of the penetration probability parameter δ. The blue filled circles are the results of MD simulations. The uncertainty in these measurements is less than the size of the markers. The RS formula given by Eq. (3.15) is shown as orange filled squares. The SIM results given by Eq. (3.20) are shown in red. The SEPC results given by Eq. (A2) are shown in dashed magenta.

1. Sequential iteration method

While Eq. (3.15) gives satisfactory results for dilute systems, as ϕ_0 is increased, the theoretical predictions show significant deviations from the simulations. Interestingly, at large ϕ_0, small perturbations from the two limits show different behavior.

As can be seen in Fig. 7, when δ is reduced slightly from the ideal limit ($\delta = 1$), the response of ϕ is small and apparently linear. Contrast this to the case where δ is increased slightly from the HR limit ($\delta = 0$) and ϕ responds with a large decrease. The nonlinear regime close to $\delta = 0$ is caused by the propensity for clusters to be in a completely overlapped state as discussed in Sec. III B.

A conjecture supported by Figs. 6 and 7 is that

$$\lim_{\phi_0 \to 1} \left. \frac{d\zeta(\delta)}{d\delta} \right|_{\delta=0} = \infty \tag{3.16}$$

and

$$\lim_{\phi_0 \to 1} \left. \frac{d\phi(\delta)}{d\delta} \right|_{\delta=0} = -\infty. \tag{3.17}$$

These findings reveal another feature of the penetrable particles: at high density, even a subtle chance to overlap will unavoidably be realized. In higher dimensional systems, we conjecture that it may even give rise to phase transitions.

To account for the nonlinear behavior of ϕ for dense systems, an expression for the volume fraction can be constructed through the sequential addition of particles. The sequential iteration method (SIM) is implemented approximately as follows: The probability that the first particle added to the system does not cover a random point A on L_x is

$$q_0 = \frac{L_x - \sigma}{L_x}. \tag{3.18}$$

Let $Q^{(n)}$ denote the conditional probability that a random point is not covered by the nth particle given $n-1$ particles have already been added (obviously, $Q^{(1)} = q_0$). Then the occupied volume fraction after adding n particles can be found as

$$\phi^{(n)} = 1 - \prod_{k=1}^{n} Q^{(k)}. \tag{3.19}$$

Within the SIM approximation, the occupied volume fraction is a function of N and the parameter δ and is calculated as

$$\phi^{\mathrm{SIM}}(N, \delta) = \phi^{(N)}. \tag{3.20}$$

The iterative procedure of calculating the values of $Q^{(k)}$ for all $k \in \{1, \ldots, N\}$ is discussed below.

When a second particle is added, then there is a chance it "does not see" the first particle because the HR interaction is not activated. If there are only two particles in the system, then their pairwise penetration probability is δ. However, for the N-particle system, the overlapping probability must obey the many-body condition and, therefore, cannot simply be equated to δ. As discussed in Sec. III B, the actual penetration coefficient ζ from Eq. (3.3) must be used in place of δ to account for multi-body effects. Thus, the probability that the second particle can overlap the first one, and does not cover point A is (ζq_0). Alternatively, when the particles do see each other, as realized with probability $(1-\zeta)$, then these particles behave as HRs. The probability that the point A is not covered by the second particle is denoted as q_1. The latter differs from q_0 since the HR interaction must be taken into account in the last case. Combining these two outcomes gives the probability of A not being covered by the second particle,

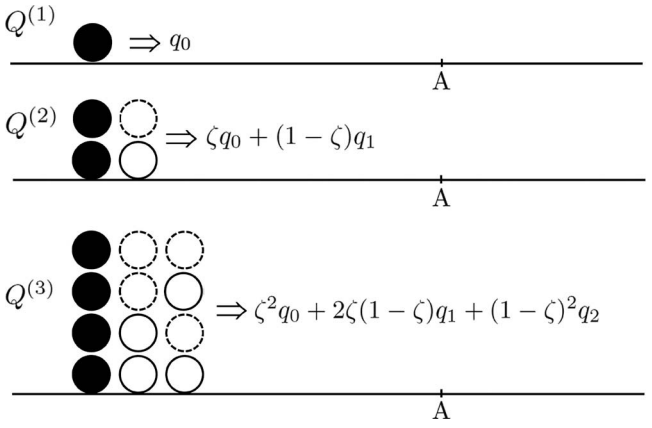

FIG. 8. A graphical representation of how the first 3 terms in the SIM are constructed. The black circle in each layer is a new added particle. The solid circles correspond to particles that have an activated HR connection with the black one. The dashed circles represent particles that are not connected with the black one (allowed to penetrate through it).

$$Q^{(2)} = \zeta q_0 + (1-\zeta)q_1. \tag{3.21}$$

Analogously, the probability that the third particle added to the system does not cover point A consists of three terms

$$Q^{(3)} = \zeta^2 q_0 + 2\zeta(1-\zeta)q_1 + (1-\zeta)^2 q_2, \tag{3.22}$$

where the first term is the probability that the HR interaction is not activated between the new and two previously placed rods, and the third rod does not cover point A; the second term is the probability that the HR interaction is activated between the third and one of two other particles, and the third rod does not cover point A; and the last term is the probability that the HR interaction is activated between the third and two other particles, and the third rod does not cover point A.

As illustrated in Fig. 8, the general probability of A not being covered by the ith particle is

$$Q^{(i)} = \sum_{k=0}^{i-1} \binom{i-1}{k} (\zeta)^{i-k-1} (1-\zeta)^k q_k, \tag{3.23}$$

where q_k is the probability point A is not covered by a new added particle given k activated particles have already been placed in the system. This probability must be defined before the expression can be evaluated.

For a new $(k+1)$-th particle added to the system, the available volume is decreased due to previously added particles. Because the actual penetration network is not known for these k particles, the volume decrease will be estimated in the mean field sense, noting that it must be proportional to the occupied volume fraction $\phi^{(k)}$, so that the available volume is $L_x - \kappa_k L_x \phi^{(k)}$, where κ_k is the coefficient of proportionality.

Therefore, analogously to Eq. (3.18),

$$q_k = \frac{L_x - \kappa_k L_x \phi^{(k)} - \sigma}{L_x - \kappa_k L_x \phi^{(k)}} = \frac{q_0 - \kappa_k \phi^{(k)}}{1 - \kappa_k \phi^{(k)}}. \tag{3.24}$$

To determine the coefficients κ_k, we note that at $\delta = 0$ the HR interactions are activated throughout the particles network, and the corresponding occupied volume fraction for the HR system is

$$\phi^{(k)} = k\sigma/L_x = k(1 - q_0). \tag{3.25}$$

On the other hand, $\zeta(0) = 0$, so that $Q^{(i)} = q_{i-1}$, and

$$\phi^{(k)} = 1 - q_0 q_1 \cdots q_{k-1}. \tag{3.26}$$

Combining these results, one obtains

$$q_0 q_1 \cdots q_{k-1} = 1 - k(1 - q_0). \tag{3.27}$$

This relation allows one to express q_k via q_0,

$$q_k = \frac{q_0 q_1 \cdots q_k}{q_0 q_1 \cdots q_{k-1}} = \frac{1 - (k+1)(1 - q_0)}{1 - k(1 - q_0)}. \tag{3.28}$$

Comparing this formula with Eq. (3.24) and taking $\phi^{(k)}$ from Eq. (3.25), one can find that all the coefficients κ_k are equal to unity, $\kappa_k = 1$, so that the recurrence relation (3.24) reads

$$q_k = \frac{q_0 - \phi^{(k)}}{1 - \phi^{(k)}}. \tag{3.29}$$

Equations (3.19), (3.20), (3.23), and (3.29) constitute the main result of this section, which connects the occupied volume fraction with the penetration probability. In the limiting cases it leads to the well known results: for $\delta = 0$,

$$\phi^{\mathrm{SIM}}(N, 0) = 1 - q_0 q_1 \cdots q_{N-1} = \frac{N\sigma}{L_x}, \tag{3.30}$$

which is the HR limit given by Eq. (3.8), and for $\delta = 1$,

$$\phi^{\mathrm{SIM}}(N, 1) = 1 - q_0^N, \tag{3.31}$$

which is the exact result given by Eq. (3.10).

The results of the SIM approximation are shown in Fig. 7. It can be seen that this method shows excellent agreement across all ranges of δ and ϕ_0, including the nonlinear regime close to $\delta = 0$ at large ϕ_0. While the RS formula fails to agree with the simulation data, the SIM appears to correct the derivation flaws present in Eq. (3.15) and thus gives a more accurate method for predicting ϕ in one-dimensional systems in which the dynamics are propagated using the SPA.

2. Iso-δ lines

It is interesting to observe ϕ as a function of ζ with overlaid lines corresponding to the constant δ values. As seen in Fig. 9, when these iso-δ lines are approximately vertical, there are small deviations between δ and ζ. Thus, the predicted overlap ratios are the same as the observed overlap ones. At these points, $g_2(r; \delta) \approx \delta$ and the RS formula of Eq. (3.15) provides good agreement with simulation. It can be conjectured that if Eq. (3.5) holds, expressions that rely on this pair correlation function value in the penetrative region can give accurate results for the occupied volume of a penetrable system.

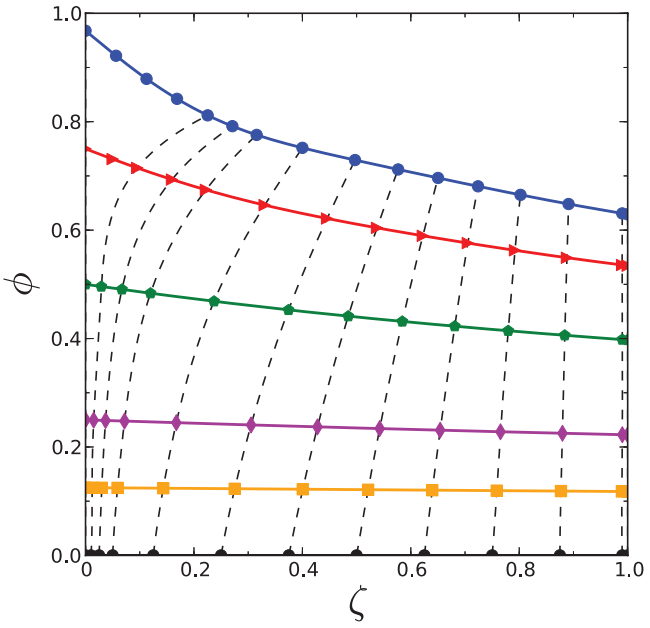

FIG. 9. Occupied volume fraction ϕ as a function of the observed penetration probability parameter ζ. The curves are indicated as in Fig. 6. The black dashed curves represent the iso-δ lines.

IV. CONCLUSIONS

In this work, we have developed a new model to simulate the dynamics of penetrable systems in one dimension through the use of a SPA. This stochastic algorithm allows the simulation of pseudo-soft matter where particles can overlap despite being governed by potentials that are unbounded at the origin. Molecular dynamics simulations of several SPA systems have been performed using stochastic collision rules. The results of these simulations have been used to measure the occupied volume of overlapping hard rods confined to move on a line. While a theoretical prediction of the occupied volume is a fundamental question, the application of theories previously developed for analogous permeable systems[53,54] fails to give agreement with the simulation results. This has necessitated the derivation of new analytical expressions for the occupied volume fraction for permeable rods satisfying the SPA. We found these to be in excellent agreement with results obtained from dynamical simulations of penetrable homogeneous systems in one dimension.

A quadrature of the penetrative region of the pair correlation function is found to be of principal importance in predicting the overlapped particle ratios and thus structural knowledge of overlap probabilities is necessary to predict the occupied volume due to the non-negligible contribution of multi-body effects at high densities. In some cases, to be presented in future work, closed form solutions for the structural properties of stochastically penetrable models are known. As such, stochastic potentials could provide a methodological framework to acquire analytic solutions to problems that are otherwise intractable when framed deterministically. Additionally, we conjecture that one-dimensional penetrable models could allow for solubility of non-penetrable models in higher dimensions when the lower dimensionality is treated as a projection from higher dimensions.

ACKNOWLEDGMENTS

This work has been partially supported by the National Science Foundation (NSF) through Grant No. NSF-CHE-1112067. The computing resources necessary for this research were provided to the Center for Computational Molecular Science and Technology by the National Science Foundation through Grant No. NSF-CHE0946869. Travel between partners was partially supported through the People Programme (Marie Curie Actions) of the European Unions Seventh Framework Programme FP7/2007-2013/ under REA Grant Agreement No. 294974.

APPENDIX: SEMI-EMPIRICAL PERTURBATIVE CORRECTION

The occupied volume fraction is well known in the limiting cases of $\delta = 0$ and $\delta = 1$ where it takes the exact forms, Eqs. (3.8) and (3.10), respectively. At small ϕ_0, where multiple particle overlaps result in small contributions to $g_2(r; \delta)$, the two limiting values are approximately additive and weighted by δ. In this low density approximation (LDA), the interpolated volume fraction is

$$\phi^{\mathrm{LDA}} = (1-\delta)\phi_0 + \delta\left(1 - \left(1 - \frac{\phi_0}{N}\right)^N\right), \tag{A1}$$

and is valid for any D. While the iterative procedure developed in Sec. III C 1 shows excellent agreement with the volume fractions obtained from simulation data, the analytic expression can be cumbersome, especially for large values of N. A focus of our future research is to understand how explicit solvent geometries affect reaction rates and molecular geometries as a chemical reaction proceeds.[56,57] As such, a simple analytic functional form is needed for use in reaction rate formulas, and so we propose a semi-empirical perturbative correction (SEPC) of Eq. (A1) where a perturbative term P_0 has been added

$$\phi^{\mathrm{SEPC}} = (1-\delta)\phi_0 + \delta\left(1 - \left(1 - \frac{\phi_0}{N}\right)^N\right) + P_0. \tag{A2}$$

To keep limiting values of ϕ unchanged, i.e., to maintain the exact limits at $\delta = 0$ and $\delta = 1$, a perturbation of the form

$$P_0 = \kappa(\phi_0)\left(\delta - \frac{1 + a(\phi_0)}{1 + a(\phi_0)\sqrt{\delta}}\sqrt{\delta}\right) \tag{A3}$$

is conjectured. It corresponds to a one-term approximation for the higher order overlap probabilities. The functions $\kappa(\phi_0)$ and $a(\phi_0)$ are calculated by fitting Eq. (A2) to the MD data and are equal to

$$\kappa(\phi_0) = 0.121\phi_0^2 + 0.266\phi_0^3 - 0.159\phi_0^4, \tag{A4}$$

$$a(\phi_0) = 0.025 + 26.14\phi_0^5 - 34.56\phi_0^6 + 33.92\phi_0^8. \tag{A5}$$

In Fig. 7, ϕ^{SEPC} is shown as a magenta dashed line.

[1] H. Graf and H. Löwen, Phys. Rev. E **57**, 5744 (1998).
[2] M. Schmidt and M. Fuchs, J. Chem. Phys. **117**, 6308 (2002).
[3] C. N. Likos, S. Rosenfeldt, N. Dingenouts, M. Ballauff, P. Lindner, N. Werner, and F. Vogtle, J. Chem. Phys. **117**, 1869 (2002).
[4] J. C. Pamies, A. Cacciuto, and D. Frenkel, J. Chem. Phys. **131**, 044514 (2009).
[5] B. Mladek, M. Fernaud, G. Kahl, and M. Neumann, Condens. Matter Phys. **8**, 135 (2005).
[6] F. Stillinger, J. Chem. Phys. **65**, 3968 (1976).
[7] C. Zachary, F. Stillinger, and S. Torquato, J. Chem. Phys. **128**, 224505 (2008).
[8] A. Ikeda and K. Miyazaki, Phys. Rev. Lett. **106**, 015701 (2011).
[9] W. Krekelberg, T. Kumar, J. Mittal, J. Errington, and T. Truskett, Phys. Rev. E **79**, 031203 (2009).
[10] C. Marquest and T. Witten, J. Phys. **50**, 1267 (1989).
[11] A. Santos and A. Malijevský, Phys. Rev. E **75**, 021201 (2007).
[12] A. Malijevský, S. Yuste, and A. Santos, Phys. Rev. E **76**, 021504 (2007).
[13] A. Malijevsky and A. Santos, J. Chem. Phys. **124**, 074508 (2006).
[14] N. Choudhury and S. Ghosh, J. Chem. Phys. **119**, 4827 (2003).
[15] L. Viererblová, J. Kolafa, S. Labík, and A. Malijevský, Phys. Chem. Chem. Phys. **12**, 254 (2010).
[16] C. Likos, M. Watzlawek, and H. Löwen, Phys. Rev. E **58**, 3135 (1998).
[17] R. Fantoni, A. Malijevsk, A. Santos, and A. Giacometti, Mol. Phys. **109**, 2723 (2011).
[18] R. Fantoni, A. Giacometti, A. Malijevský, and A. Santos, J. Chem. Phys. **131**, 124106 (2009).
[19] A. Santos, R. Fantoni, and A. Giacometti, Phys. Rev. E **77**, 051206 (2008).
[20] S. Suh, C. Kim, S. Kim, and A. Santos, Phys. Rev. E **82**, 051202 (2010).
[21] Y. Chiew and E. Glandt, J. Colloid Interface Sci. **99**, 86 (1984).
[22] J. Quintanilla and S. Torquato, Phys. Rev. E **54**, 4027 (1996).
[23] S. Torquato and G. Stell, J. Chem. Phys. **80**, 878 (1984).
[24] J. Quintanilla and S. Torquato, Phys. Rev. E **54**, 5331 (1996).
[25] B. Widom, J. Chem. Phys. **54**, 3950 (1971).
[26] S. Torquato and G. Stell, J. Chem. Phys. **79**, 1505 (1983).
[27] K. Gotoh, M. Nakagawa, M. Furuuchi, and A. Yoshigi, J. Chem. Phys. **85**, 3078 (1986).
[28] S. Torquato, *Random Heterogenous Materials: Microstructure and Macroscopic Properties* (Springer-Verlag, New York, 2002).
[29] S. Suh, W. Min, and J. MacElroy, Bull. Korean Chem. Soc. **20**, 1521 (1999).
[30] S. Lee and S. Torquato, J. Chem. Phys. **89**, 3258 (1988).
[31] M.-J. Fernaud, E. Lomba, and L. L. Lee, J. Chem. Phys. **112**, 810 (2000).
[32] S. Kim and S. Suh, J. Chem. Phys. **117**, 9880 (2002).
[33] L. Blum and G. Stell, J. Chem. Phys. **71**, 42 (1979).
[34] E. Barkai and V. Fleurov, J. Stat. Phys. **96**, 325 (1999).
[35] E. Barkai, V. Fleurov, and J. Klafter, Phys. Rev. E **61**, 1164 (2000).
[36] J. Dorfman, M. Ernst, and D. Jacobs, J. Stat. Phys. **81**, 497 (1995).
[37] M. Ernst and P. Binder, J. Stat. Phys. **51**, 981 (1988).
[38] D. Chandler, J. Weeks, and H. Andersen, Science **220**, 787 (1983).
[39] A. V. Popov, J. Melvin, and R. Hernandez, J. Phys. Chem. A **110**, 1635 (2006).
[40] A. K. Tucker and R. Hernandez, J. Phys. Chem. B **116**, 1328 (2012).
[41] A. Santos, Phys. Rev. E **86**, 040102(R) (2012).
[42] L. Tonks, Phys. Rev. **50**, 955 (1936).
[43] I. Bena, C. Van den Broeck, and R. Kawai, Europhys. Lett. **71**, 879 (2005).
[44] L. Van Hove, Physica **16**, 137 (1950).
[45] M. P. Allen and D. J. Tildesley, *Computer Simulations of Liquids* (Oxford, New York, 1987).
[46] A. Elsner, A. Wagner, T. Aste, H. Hermann, and D. Stoyan, J. Phys. Chem. B **113**, 7780 (2009).
[47] U. Brodatzki and K. Mecke, Comput. Phys. Commun. **147**, 218 (2002).
[48] M. Bishop and B. Berne, J. Chem. Phys. **60**, 893 (1974).
[49] J. Haus and H. Raveché, J. Chem. Phys. **68**, 4969 (1978).
[50] Z. Salsburg, R. Zwanzig, and J. Kirkwood, J. Chem. Phys. **21**, 1098 (1953).
[51] M. Bishop, M. Derosa, and J. Lalli, J. Stat. Phys. **25**, 229 (1981).
[52] J. Kirkwood, J. Chem. Phys. **3**, 300 (1935).
[53] P. Rikvold and G. Stell, J. Colloid Interface Sci. **108**, 158 (1985).
[54] P. Rikvold and G. Stell, J. Chem. Phys. **82**, 1014 (1985).
[55] S. Torquato, B. Lu, and J. Rubinstein, Phys. Rev. A **41**, 2059 (1990).
[56] T. Bartsch, T. Uzer, and R. Hernandez, J. Chem. Phys. **123**, 204102 (2005).
[57] R. Hernandez, T. Bartsch, and T. Uzer, Chem. Phys. **370**, 270 (2010).